Real-Time Pore Blockage Quantification in Hydropower Drainage Pump Inlets via Canny Edge Detection and HSV Segmentation

Xiangqian Fu[1, 2], Linghua Hou[3, *], Qiqi Ding[4] and Long Xu[4]
[1] Hubei Technology Innovation Center for Smart Hydropower, Wuhan 430000, China
[2] School of Power and Mechanical Engineering, Wuhan University, Wuhan 430000, China
[3] China Yangtze Power Co., Ltd., Beijing 100032, China
[4] Three Gorges Jinshajiang Chuanyun Hydropower Development Co., LTD. Yongshan Xi Luodu Power Plant, Yongshan 657300, China
E-mail: houlinghua123@126.com
[*]Corresponding author

Keywords: drainage pump unit, edge extraction, HSV color detection, scale, small pore filter

Received: April 25, 2025

As a core component of the diversion tunnel in hydropower stations, the drainage pump is prone to blockage in its inlet filter due to severe water calcification inside the tunnel. In this study, the present study proposes a computer-vision-based detection method to assess the blockage degree of the inlet filter's pores. Specifically, the outline of the small pores in the inlet screen of the drainage pump unit was captured using the Canny edge detection algorithm. Then the pore and non-pore areas of the filter were distinguished with the HSV color model. Finally, the degree of blockage was determined by calculating the proportion of pore areas within the filter screen. When applied to a real hydropower station using 12 images sampled at 15-day intervals, this developed computer vision technology achieved 13.6% average error against manual annotations and demonstrated real-time processing (<1s/image on 4-core/8GB edge devices) effective detection for the pores blockage degree of the drainage pump's inlet filter screen, by quantitatively assessing the blockage degree, it provides critical metrics that enable predictive maintenance scheduling and performance evaluation, thereby ensuring reliable hydraulic performance and minimizing downtime in the hydropower station's drainage system.

Povzetek: Predstavljena je hibridno računalniško-vidna metoda s Canny robnim zaznavanjem in HSV segmentacijo za sprotno kvantifikacijo zamašitve por na črpalkah, ki omogoča prediktivno vzdrževanje hidroenergetskih sistemov.

1 Introduction

As one of the most essential parts of drainage systems, drainage pump unit is widely used in hydropower stations, mines, rivers and other fields for water management [1]. Because of the special landform and the low terrain height in southwest region of China, the powerhouse for large hydropower station is mostly located in the riverside mountains. To deal with the accidents such as water seepage from the mountain and heavy rainfall, etc., which can lead to flooding of the powerhouse, the hydropower station is often equipped with a comprehensive drainage system to discharge the accumulated water. Usually, the seepage water from the mountain is diverted to the catchment area through the open channel, and then the water is discharged through the drainage pump unit. But drainage pump unit may be damaged during this process because of inhalation of debris from the mountain or water calcification. Water calcification stems from calcium carbonate (CaCO3) precipitation in groundwater, driven by temperature shifts and pH changes. Southwest China's karst geology exacerbates mineral dissolution, while debris like silt combines with scales to form dense fouling layers, accelerating pore blockage. Such blockages significantly increase hydraulic resistance, forcing pumps to overwork, elevating energy consumption and overheating risks. Prolonged operation may cause motor burnout, while partial drainage raises flood risks during storms. Nowadays, people add a filter screen to the inlet channel of the drainage pump unit to avoid the damage but the small pores of the filter screen are still easily blocked by calcified debris, resulting in reduced hydraulic performance of the drainage pump unit and even leading to motor damage. Although the electrical submersible pump has been in use for many years, there are still many problems which can be summarized into three main categories: electrical problems, mechanical problems and operational problems. For operational problems, fluid with different nature would cause different problems with multi-phase fluids (liquids, solids and gases) causing more serious problems than others [2].

In drainage systems, traditional blockage detection methods such as pressure differential monitoring, vibration analysis, and acoustic emission sensing often lack spatial resolution, making it challenging to quantify pore-level obstructions. Recent advancements in computer vision have enabled non-invasive inspection techniques. For instance, an AIoT-based real-time visual detection solution

for culvert blockages integrates artificial intelligence, computer vision, and edge computing to effectively assess blockage status. However, these methods often rely on extensive training data or perform inadequately under dynamic environmental conditions, such as fluctuating illumination in enclosed hydropower tunnels. Notably, research addressing calcification-induced pore blockages in hydropower drainage systems is limited. One study applied impedance spectroscopy and tomography to monitor calcite deposits in drainage pipes, providing insights into the formation and detection of such blockages [3]. However, integrating real-time visual monitoring with predictive models remains underexplored. Traditional RGB-based vision systems often misclassify calcified deposits due to color similarities with filter materials. In contrast, utilizing alternative color spaces and edge detection algorithms has shown potential in distinguishing mineral deposits from metallic surfaces, yet their application in hydropower pump filters has not been fully investigated [4].

Moreover, existing methods-including manual inspections, predictive models, and traditional computer vision-face three key limitations: (1) labor-intensive periodic cleaning cannot address sudden blockages; (2) data-driven models require extensive datasets and calibration, hindering deployment in variable environments; and (3) conventional vision systems struggle with lighting fluctuations and color ambiguities between scale deposits and pores. To overcome these gaps, we propose a hybrid computer vision framework combining Canny edge detection and HSV segmentation. This approach bypasses the dependency on training data by directly quantifying pore geometry and color contrast, ensuring robustness in enclosed tunnels with dynamic conditions. Real-time porosity monitoring enables predictive maintenance, surpassing the reactive nature of traditional manual strategies. To contextualize our approach, Table 1 compares mainstream blockage detection methods across five critical dimensions:

Table 1: Comparative analysis of blockage detection methods

Method	Required Data	Resolution	Robustness	Cost	Deployment Context
Pressure differential	Sensor readings	Low	Flow-dependent	Medium	Pipe systems
Impedance tomography	Electrochemical signals	Medium	Contact-required	High	Lab/small pipes
AIoT vision	Labeled image datasets	High	Lighting-sensitive	High	Open culverts
RGB analysis	RGB images	Medium	Color-ambiguous	Low	Controlled lighting
Our method	Single unlabeled image	High	Lighting-adaptive	Low	Enclosed tunnels

Currently, different preventive and control measures are adopted to solve the problem of flow channel blockage for actual working places. For example, for irrigation canals, pumping stations, inlet sluice, and other hydraulic structures, Singal et al. [5] added garbage racks in front of the water intakes to prevent floating and sinking objects from causing damage or running problems to the turbines and other components. Hribernik [6] used hydropower station flow and waste rack head losses to build rack clogging models to distinguish head losses caused by debris and rack structures. Cui et al. [7] found that groundwater along rivers and lakes showed a periodic change and then did relevant experiments to evaluate the effect of water level changes on the migratory depositional characteristics of particles in porous media. Tao et al. [8] designed a pre-pumped micro pressure filter to filter sediment particles through a stainless-steel filter and developed a prediction model for filter head loss. Liu et al. [9] developed a novel simulation model which coupled hydrodynamics and hydrochemistry for calculating the deposition rate of CaCO3 fouling in the pipeline surface. Ogie et al. [10] proposed a method for measuring and ranking the vulnerability of pumping stations to trash blockage, which makes it possible to point out the pumping stations that are most vulnerable to trash blockage. For instance, Rana et al. [11] found in the ultrafiltration analysis and comparison of produced water in the upstream oil and gas operations that the best membrane for treating produced water was zirconium oxide. Fujita et al. [12] tested the Fe removal capacity of three green filtration materials in deployed closed- and open-loop thermal systems using groundwater geothermal energy (GGE) to reduce clogging problems in open-loop ground source heat pump systems. Nallakukkala et al. [13] proposed three techniques for controlling scale formation: removal or decrease of Scale-forming species, water treatment for acidification of feed and degassing CO2 generated from carbonates, and chemical treatment for descaling using acids or chelating agents.

The above research focuses on analyzing the flow pattern, the clogging mechanism and flow channel structure design to cope with flow channel blockage. Although few studies have constructed predictive models for the blockage degree of flow channel, these methods are all built based on being able to accurately extract blockage-related operation and environment variables, as well as

sufficient high-quality positive and negative blockage training sample data sets, which makes the modal hard to be applied in special work places such as the diversion tunnel's catchment area of hydropower station, where the water calcification is unavoidable and the optimization of the inlet filter structure of the pump is limited. Therefore, it is necessary to detect the blockage in these work places in advance. In this study, the present study proposes a computer-vision-based detection method for the blockage degree in the inlet filter's pores. High-definition cameras were installed to collect images of drainage pump units periodically, and then Canny edge detection algorithm was used to extract the pores outline of the inlet filter screen in this image. Finally, the HSV color model was used to separate the pore space from the non-pores space (including limescale and filter screen body). The proportion of pore areas in the filter screen was calculated, and the remaining porosity ratio threshold alarm was set to notify the relevant personnel in advance to carry out the filter screen descaling treatment.

To reliably quantify pore blockage in hydropower drainage pumps under dynamic tunnel conditions, our approach combines:

(1) Canny edge detection for robust pore localization;

(2) HSV segmentation to distinguish calcified deposits;

(3) Pore-area calculation for blockage quantification;

Compared with the manually annotated results, the accuracy of the algorithm model was verified through error comparison.

Main Contributions:

Hybrid vision framework: Combined Canny edge detection and HSV segmentation to quantify pore blockage, overcoming limitations of manual inspections and data-driven models.

Training-free real-time monitoring: Enabled robust pore detection in dynamic tunnel environments without requiring large datasets.

Practical validation in hydropower stations: Tracked pore-area reduction over time, supporting predictive maintenance and downtime reduction.

Enhanced robustness via HSV: Outperformed RGB methods in distinguishing pores from calcified deposits under variable lighting.

1 Methods

2.1 Canny edge detection

As a general edge detection algorithm [14], the Canny algorithm can detect the edge in a very robust way. It can extract the image edges without disturbing the image features and separate the noise from the input image. It is one of the most practical and functional detection operators available. The basic idea of the Canny algorithm is to use a two-dimensional Gaussian filter template to smooth the image, then use the derivative algorithm to find the grayscale gradient of the pixel in the x and y direction and further calculates the gradient's magnitude. Then it carries out the 'non-maximum suppression' to find out the maximum value of the pixel in the gradient direction and determine whether the central pixel is tentatively set as an edge point. Finally, it conducted the double-threshold selection to make a final judgment on the tentative edge points obtained in the previous step and select the final edge.

2.1.1 Gaussian filter

In the data acquisition stage, the digital image acquired by the sensor is usually affected by noise, and image denoising can effectively preserve the image edge and get better expansion in the flat area [15]. Gaussian filters are good at removing normally distributed noise, which is usually found in cameras images produced through its digitization process. It is a natural phenomenon caused by the light-reflecting nature of the camera itself and the sensitivity of the optical sensor [16].

First, the image noise is removed by a filter through convolving with the image. The noise in the image corresponds to the high-frequency part of the image so that the noise can be removed in the frequency domain. However, edge detection and filtering usually conflict with each other because the filtered image is pixel-weighted averaged according to the template, which reduces noise but blurs the image edge simultaneously, resulting in increasing uncertainty of edge position. Hence, compromise between the two is necessary. The kernel determined by Gaussian function can resist noise interference while not affect the sensitivity of edge detection too much. That's the reason why we choose Gaussian filter to remove the noise in the digital image. The 2D Gaussian kernel is defined as follows:

$$K = \frac{1}{2\pi\sigma^2} exp\left(-\frac{x^2+y^2}{2\sigma^2}\right) \quad (1)$$

2.1.2 Intensity and direction of pixel gradient

The image edge can be in any direction. The gradient (G) magnitude and the direction (θ) of each pixel point can be obtained by calculating the first derivative of the horizontal and vertical directions of each pixel point. The G and θ can be calculated as follows:

$$G = \sqrt{G_x^2 + G_y^2} \quad (2)$$

$$\theta = arctan\left(\frac{Gy}{Gx}\right) \quad (3)$$

The first derivative of the horizontal and vertical gradients can be calculated by operator filtering such as Roberts, Prewitt, and Sobel. Among them, the Sobel operator is particularly useful for image processing and edge computing [17]. Therefore, this paper used the Sobel operator instead of the traditional 2*2 template to reduce the generation of isolated edge points and pseudo-edge points. The Sobel operator gave more weight on the center coefficient, which can provide smoother images. The gradient operator of Sobel along the x and y directions are calculated as follows:

$$g_x = \begin{bmatrix} -1 & 0 & 1 \\ -2 & 0 & 2 \\ -1 & 0 & 1 \end{bmatrix} \quad (4)$$

$$g_y = \begin{bmatrix} -1 & -2 & 1 \\ 0 & 0 & 0 \\ 1 & 2 & 1 \end{bmatrix} \quad (5)$$

2.1.3 Non-Maximum Suppression

The Non-maximum Suppression (NMS) was first created in edge detection field to improve a rough edge response to a thin line [18]. This oriented NMS operates in a one-dimensional (1-D) range perpendicular to the edge. Kitchen and Rosenfeld [19] extended this concept to isotropic NMS to locate two-dimensional (2-D) characteristic points of an image, which are selected as local maxima of an "Angle" image over a neighborhood.

Non-maximum suppression searches for local gradient maxima of pixel points along the direction of the pixel gradient and sets the gray value of pixel points corresponding to local non-maxima to 0. Its function is to remove false edges and refine and precisely locate the image edges.

2.1.4 Dual Threshold Selection

By setting two thresholds TH1 and TH2 (TH1 > TH2), double threshold selection filters the local maximum pixel x generated in non-maximum suppression to realize noise reduction and edge continuity. In this process, the pixel points are filtered into three sets: the strong edge set S_s, the weak edge set S_w, and the abandoned edge set S_d, defined as follows:

$$\{S_w | TH1 > x > TH2\} \quad (6)$$

$$\{S_s | x > TH1\} \quad (7)$$

$$\{S_d | TH2 > x\} \quad (8)$$

When its gradient is larger than TH1, the pixel point is classified as "definite edge" pixel and are retained. Pixel points with gradients smaller than TH2 are regarded not to be edges and are discarded. For those Pixel points whose gradient is between TH1 and TH2, they are considered to be part of the edge only if they are connected to a "definite edge" pixel point, otherwise they are discarded.

2.2 HSV color space

HSV (Hue, Saturation, Value) is created by graphic designers mimicking the process of artists creating colors [20-21]. H (hue) represents the hue of a pixel point, and is measured by Angle with value ranges from 0° to 360°. S (saturation) represents the saturation of the pixel point, and its saturation value ranges from 0 to 255. V (value) represents the brightness of the pixel point, reflecting the colorless concept of intensity. The value of V ranges between 0.0~1.0, with 0.0 representing black and 1.0 denoting white.

HSV aggregations are closer to human vision (as they reached highest F1 values) than the RGB aggregations, and HSV aggregations have lower standard deviations than RGBs, suggesting that the HSV methods are more robust [22]. As the HSV model is evolved from the RGB cube model, so the HSV color space can be converted from the RGB color space. Based on the principle of its conversion, the HSV color space can be calculated through the following formula:

$$H = \begin{cases} arccos\left(\dfrac{(R-G)+(R-B)}{2\sqrt{(R-G)^2+(R-B)(G-B)}}\right), B \le G \\ 2\pi - arccos\left(\dfrac{(R-G)+(R-B)}{2\sqrt{(R-G)^2+(R-B)(G-B)}}\right), B > G \end{cases} \quad (9)$$

$$S = \frac{max(R,G,B) - min(R,G,B)}{max(R,G,B)} \quad (10)$$

$$V = \frac{max(R,G,B)}{255} \quad (11)$$

where, *R*, *G*, and *B* are the three components of the RGB model, respectively.

2 Results

Applied this developed computer vision technology to the drainage pump of a real hydropower station. The pump was installed vertically with a filter screen at the inlet for filtering debris and calcified matter. A camera was installed on the wall of the catchment area closest to the pump. The pore blockage detection of the inlet filter included three steps: filter profile extraction, HSV separation of filter's small pores and pore area calculation.

2.1 Inlet filter profile extraction

The extraction steps of the inlet filter are as follows:

a. Marking the outline of inlet filter. The edge outline of the inlet filter was manually marked with Anylabeling tool to get the (x, y) coordinate of these pixel points. The image taken from the camera is shown in Fig. 1a.

b. Transforming into mask area. Read the profile coordinates of the inlet filter in json file and transform them into masked regions based on OpenCV as shown in Fig. 1b.

c. Filling the mask area. Actual pictures of the filter were used to fill the mask area obtained, and the area out of the profile was further filled with white

color. Finally, the complete outline picture of the filter screen was obtained, as shown in Fig. 1c.

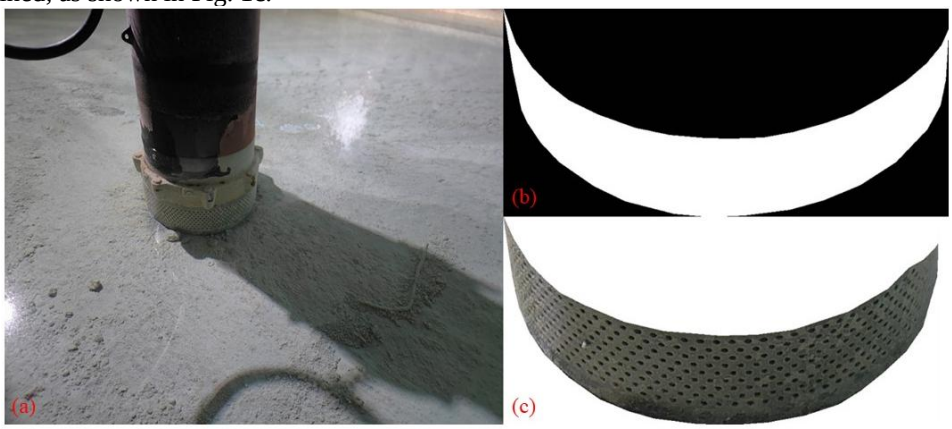

Figure 1: Extraction process of intake filter

3.2 Identification of filter's pores with HSV

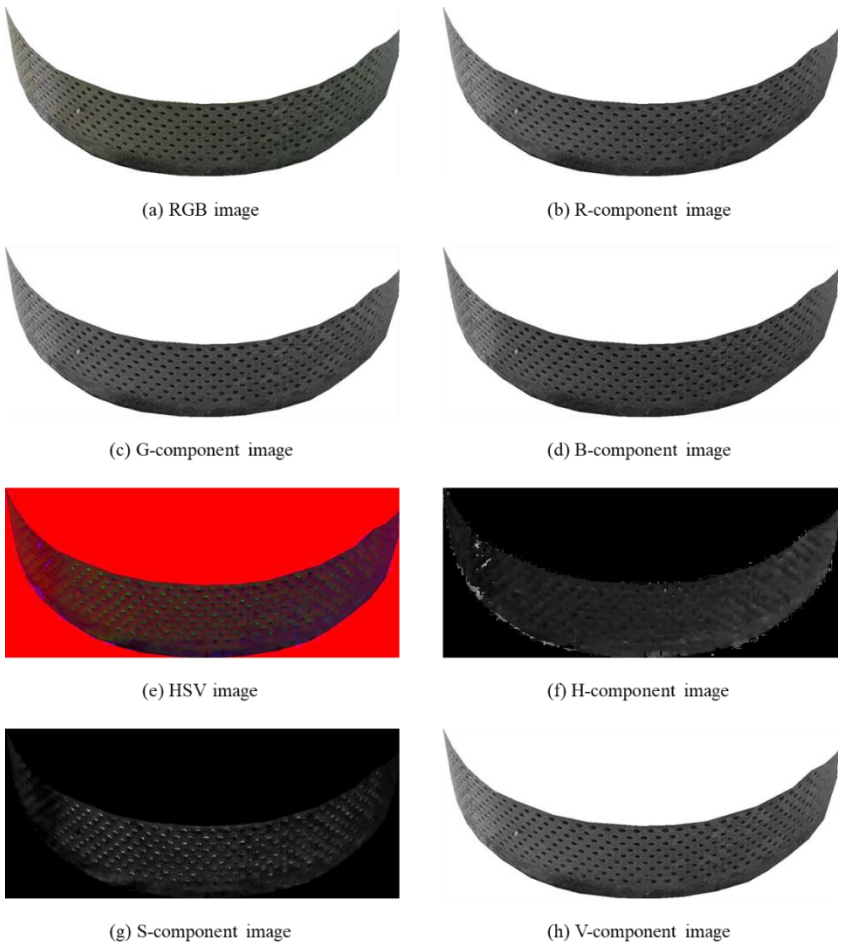

Figure 2: HSV result of RGB conversion of intake filter

The RGB component of the inlet filter' image was obtained first, and then they were converted into HSV component according to the Eq. (9-10). During the conversion process, the thresholds of hue, saturation, and brightness needed to be adjusted to enhance the filter screen pores' characteristics. The conversion results are shown in Fig. 2.

As can be seen from Fig. 2, the RGB component diagram cannot clearly distinguish the porous area of the inlet screen from other areas while the S-component map of HSV showed clearer pore areas. Based on the HSV color, the porous regions of the filter screen were extracted, and the outline of filter's pores was further obtained through color region mask. The results are shown in Fig. 3.

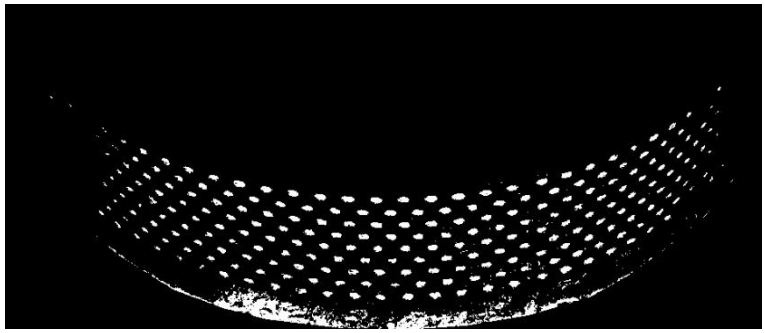

Figure 3: Mask image of filter pores

3.3 Pore area calculation

Based on the pore mask of the filter screen obtained through HSV color model, the edge of the pores was further detected by Canny algorithm. After grayscale treatment of the image, Canny operator was used to perform Gaussian filtering, gradient calculation, non-maximum suppression processing and double threshold selection. As there were many irregular lines in the picture, the key of the algorithm was the selection of the double threshold. In this study, the trackbar of OpenCV was used to dynamically adjust the dual thresholds and select the appropriate threshold combination pattern.

As there were some interference areas with similar color to the inlet screen pores, so it is necessary to further evaluate and select the pore areas obtained. In this paper, the box plot was adopted for screening. The anomalies of pore areas in the box plot were shown in Fig. 4. The y axis of the box plot represented the pixel area size, and the x axis represented the target pore area groups.

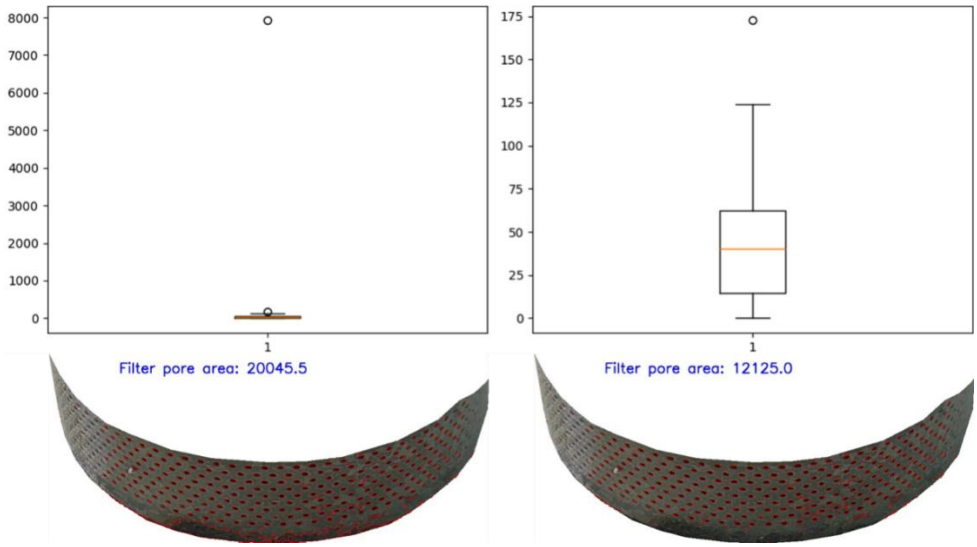

(a) (b)

Figure 4: Abnormal area box plot

As shown in Fig. 4a, there were large values in the pore area aggregation, resulting in the bad performance of the boxplot. Moreover, these outliers belonged to the non-porous area of the inlet filter screen, so they were supposed to be excluded. Fig. 4(b) showed the box plot with an area less than 1000 after excluding the outliers. The abnormal values in this box plot were the pore-connected regions, which should not be removed. There were also some small area values in the box plot which belonged to the non-pore areas as shown in Fig. 4, so further screening was required.

The values indicating small pore area mostly appeared in the lower quartile of the box plot, and the lower quartile was calculated to be 14.5. Therefore, the pore area value less than or equal to 14.5 was extracted. The diagram of screen result for the specific pore area is shown in Fig. 5.

Figure 5: Area <= 14.5 pore set

In Fig. 5, the red dot circled in green represented the non-porous area, indicating a lot of the non-porous regions having a pore area less than or equal to 14.5. Therefore, it is reasonable to use the lower quartile value for screening.

Based on the area screening results of the box plot, the S-component distance between pixels in the image was further calculated, and all pixels can be classified into two types: the pixel corresponding to the filter screen pores (the white highlights in the image) and other black regions. By accumulating the area values of the first type of pixel points, the pixel area of the filter screen pores can be obtained as 11949.5 (Fig. 6).

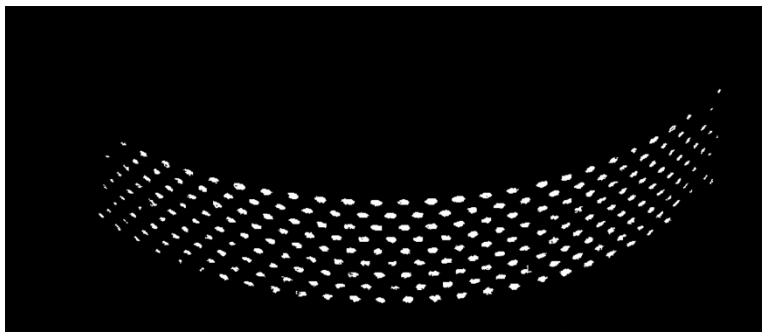

Figure 6: Exclusion of abnormal areas

To quantify detection accuracy, a benchmark was established through manual annotation. Three images with maximal temporal spans were processed as follows:

(1) Automated pore segmentation via ImageJ v1.54g Flood Fill (8-connected) failed due to region fragmentation caused by discontinuous intensity gradients;

(2) Freehand Selections were subsequently employed to trace irregular pore boundaries;

(3) Pixel areas were computed automatically using Analyze > Measure. An annotation example is shown in Fig. 7.

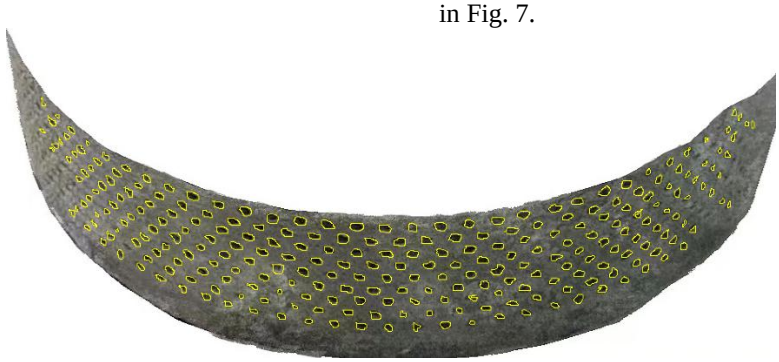

Figure 7: Manual pore annotation using ImageJ Freehand Selections

Comparing algorithmic outputs against manual benchmarks, the mean error rate of the HSV-S component reached 13.6% (Table 2), confirming detection reliability.

Table 2: Error rates (%) of pore area between manual annotation and algorithmic detection across three sample images

Sample Date	HSV-H	HSV-S	HSV-V	RGB-R	RGB-G	RGB-B
2024-01-07	24.7	12.3	19.8	18.6	19.1	19
2024-04-06	27.1	14.5	23.6	24.1	23.8	23.8
2024-06-20	29.4	13.9	25.1	24.2	22.1	23.9
Mean Error	27.1	13.6	22.8	22.3	21.7	22.2

3.4 Time variation of pore area

To verify the practicability of this study, the changes of the inlet filter over time were tracked. Real pictures of the pump unit were taken every 15 days within half a year, and the area of the inlet filter was extracted. The specific changes of the inlet filter over time are shown in Fig. 8.

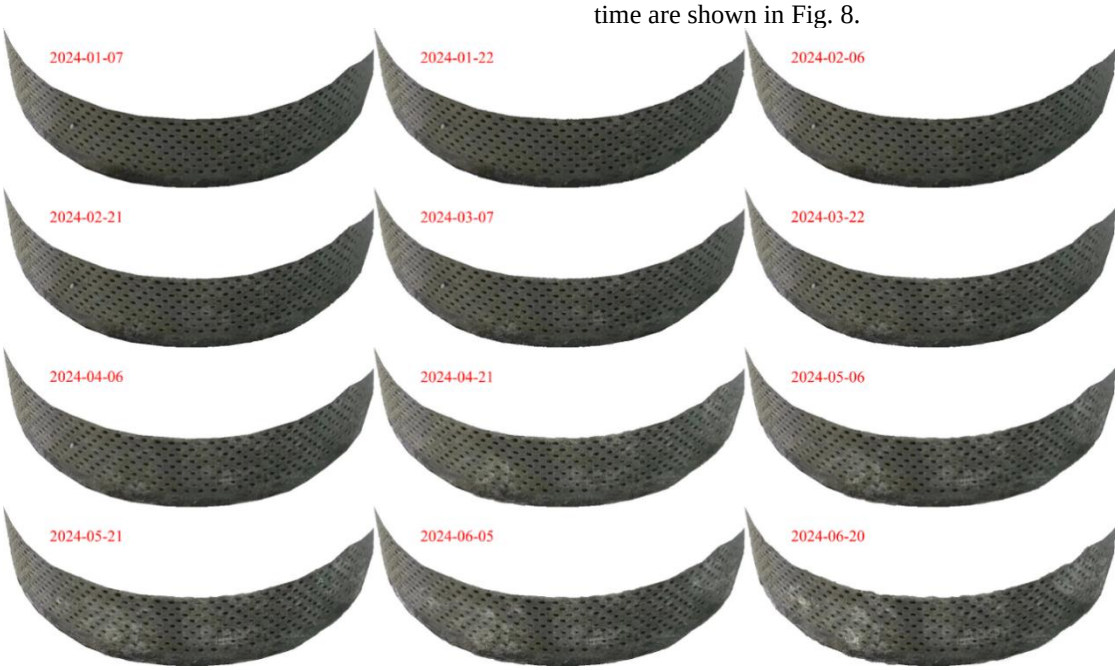

Figure 8: Changes in intake filter over time

Extract the small pore areas of the inlet filter screen in each time and figure out the small pore area. In this paper, the extraction result in different time periods was shown in the form of mask pictures to see its changes more clearly. The specific changes of the pore areas of the inlet filter screen over time are shown in Fig. 9.

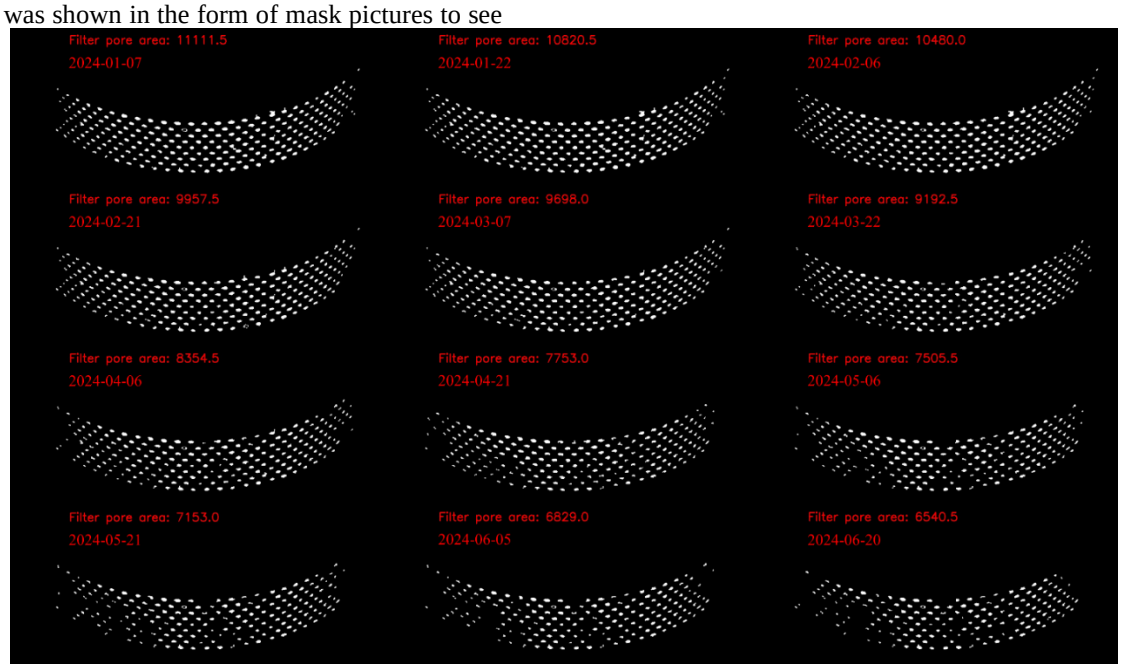

Figure 9: Intake filter pore areas over time

In Fig. 9, higher degree of blockage of the small pores were seen in the lower region of the intake filter screen than that of the upper part, which was because the impurities in the water were gathered in the lower region after precipitation, resulting in the easy blockage of the pores below the intake filter screen. The change of pore area of the filter over time can be shown clearly by plotting the curve of pore area versus time. The specific inlet filter screen pore area with time change curve is shown in Fig. 10. It's clear that the pore area of the inlet filter screen was getting smaller and smaller over time leading to the pore blockage of the inlet filter later, which would affect the running of the pump unit. This study realizes the real-time monitoring of the inlet filter screen's pore areas, providing a basis for the reasonable arrangement of cleaning work, and timely reflecting the serious blockage of the pump unit.

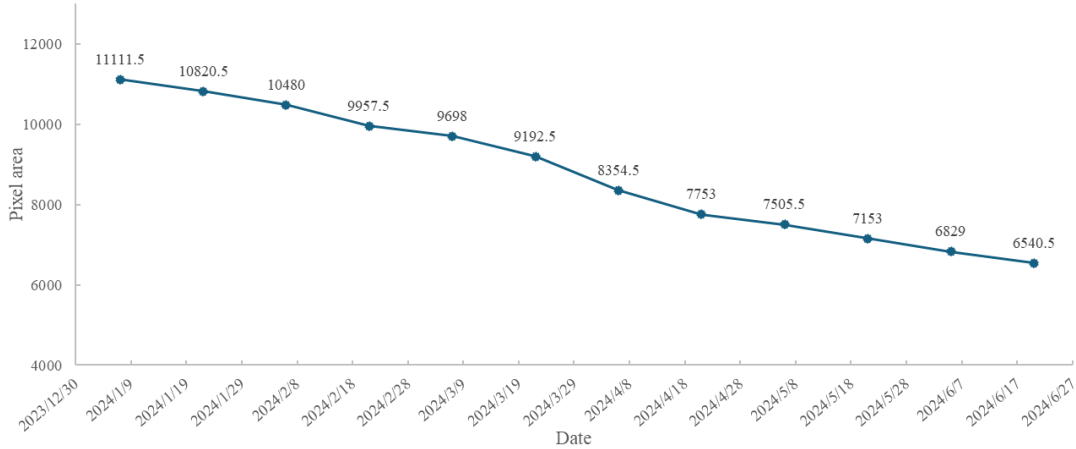

Figure 10: Intake filter pore area versus time curve

3 Discussion

This study aimed to provide a set of low-cost practical scheme for monitoring the blockage of the inlet filter screen of the drainage pump unit of the diversion tunnel of the hydropower station. This study comprehensively analyzed the previous research and practice solutions, such as the use of garbage racks and the improvement of filtering devices, but they were still needed to be cleaned regularly to prevent blockage. This study results also have some reference value for similar engineering applications. First, the computer vision technology was applied to optimize the manual regular cleaning plan. As the water calcification and the remote location of diversion tunnel which was far away from the management area, the regular cleaning program was still used. This program resulted in unable to clean the sudden blockage problem timely and multiple failures of the pump unit. Compared with regular cleaning programs, computer vision technology can monitor abnormal conditions timely such as sudden blockage and accelerated scaling. Moreover, it offers advantages including simple operation, low cost, and attractive performance [23]. Although the severe calcification of water in diversion tunnel, the calcified matter would precipitate to the bottom, so the water surface above is relatively clear. Besides, the diversion tunnel is enclosed space and is illuminated by searchlights throughout the year, which ensures that the brightness of the light is constant and the camera provides consistent imaging the inlet filter under the water. The camera is waterproof and dustproof with IP66 and above to prevent water from flooding the camera.

For the recognition object of computer vision, instead of direct recognition of the scaling region of inlet filter, we choose to recognize the small pore region of inlet filter. While the former enables intuitive assessment of blockage scale on the inlet filter, it achieves substantially reduced computational complexity, this does not effectively represent the blockage degree of the filter screen in drainage pump because serious scaling in other non-porous areas of the inlet filter does not mean that the pump unit is in a blocked state. If the staff only cleans the blockage of the small pore of the water inlet filter, the former would still determine that the pump unit is in a blocked state, leading to the erroneous diagnostics. In our study, we combine Canny algorithm with HSV color model to extract a clear image of the porous area of the inlet filter screen. Canny has excellent performance in edge detection and has been practically applied in many business fields [24-26]. We adopted the HSV model rather than the RGB model as the color extraction scheme because the extraction of the RGB scheme in the small pore area of the inlet filter is not ideal and the HSV color extraction scheme provides superior stability.

Future research mainly focuses on the in-depth analysis of the anomaly problem and further development of this study. Several practical limitations require consideration:

(1) Lighting stability in enclosed tunnels may affect edge detection consistency;

(2) Manual mask initialization is currently required for filter localization;

(3) Water turbulence could introduce transient noise in pore identification;

(4) With water level changes, light refraction variations may influence pore area measurements;

(5) Potential color similarity between scale deposits and pore areas may challenge extraction accuracy.

4 Conclusions

In this study, the profile mask of the inlet filter screen of the pump was selected with manual marks to extract the complete profile picture of the filter screen. Then, HSV color model was used to extract the S component which can separate the pores of the filter from non-porous areas. Finally, the pixels of the S-component map of the filter screen were classified by color Euclide distance, and the non-porous regions of the inlet filter screen were removed so that the pore pixel area was obtained by summing up the pixels representing the pores of the filter screen. By calculating the pore pixel area of the filter screen regularly and sending the result to the control room of the hydropower station, the dynamic tracking and monitoring of the blockage degree of the inlet filter screen of the pump can be realized.

Acknowledgment

This work was supported by the Open Research Fund Program of Hubei Technology Innovation Center for Smart Hydropower (1523020038).

Author contributions

Xiangqian Fu: Conceptualization, Data interpretation, Writing – original draft. Linghua Hou, Qiqi Ding and Long Xu: Supervision, Data interpretation, Writing – review & editing. Xiangqian Fu: Funding acquisition. Xiangqian Fu and Linghua Hou: Conceptualization, Supervision. All authors read and approved the final version.

Conflict of interests

All authors declare no conflict of interests.

Data availability statement

The data used to support the findings of this study are all in the manuscript.

References

[1] Esmaeilpour, M., E. Nomigolzar, M. R. F. Derakhshi, and Z. Shukur. (2011) Fault diagnostics of centrifuge pump using data analysis in spectrometric method, *Informatica*, vol. 35, pp. 259-268.

[2] Kannaujia, V., S. P. Bhore and H. S. Goyal. (2024) Failure analysis of submersible pumps-A review. In: Ghoshal, S.K., Samantaray, A.K., Bandyopadhyay, S. (eds) Recent advances in industrial machines and mechanisms. IPROMM 2022. *Lecture Notes in Mechanical Engineering*. Springer, Singapore. https://doi.org/10.1007/978-981-99-4270-1_40

[3] Affortunati, S. and B. G. Zagar. (2022) Application of impedance spectroscopy and tomography to monitor calcite deposits in drainage pipes, *Elektrotechnik & Informationstechnik*, vol. 139, pp. 524-534, 2022, https://doi.org/10.1007/s00502-022-01058-5

[4] Iqbal, U., J. Barthelemy, W. Li and P. Perez. (2021) Automating visual blockage classification of culverts with deep learning, *Applied Sciences*, vol. 11, no. 16, pp. 7561, 2021, https://doi.org/10.3390/app11167561.

[5] Singal, S. K., V. Gupta and M. Sood. (2022) A Numerical study to determine the impact of trash rack blockage on head loss, *Water and Energy International*, vol. 65, no. 7, pp. 6-11.

[6] Hribernik, A. (2020) Evaluation of clogged hydropower plant trash rack losses, *Journal of Mechanical Engineering*, vol. 66, no. 2. https://doi.org/10.5545/sv-jme.2019.6313

[7] Cui, X., T. Wen, J. Li, D. Wu, Y. Fan, Y. Jin et al. (2022) Migration and deposition characteristics of particles in sand layers with fluctuating water levels, *Water, Air, & Soil Pollution*, vol. 233, no. 4, pp. n.p. https://doi.org/10.1007/s11270-022-05603-y

[8] Tao, H., Z. Wu, Y. Zhou et al. (2023) Establishment of a dimensional analysis-based prediction model for the head loss of pre-pump micro-pressure filters for micro-irrigation, *Irrigation Science*, vol. 41, pp. 803-815. https://doi.org/10.1007/s00271-023-00879-2

[9] Liu, D. G., Y. Yang, C. J. Mao et al. (2022) A Comparative study on hydrodynamics and hydrochemistry coupled simulations of drainage pipe crystallization blockage in karst tunnels, *Journal of Earth Science*, vol. 33, pp. 1179-1189. https://doi.org/10.1007/s12583-022-1720-3

[10] Ogie, R. I., S. Dunn, T. Holderness and E. Turpin. (2017) Assessing the vulnerability of pumping stations to trash blockage in coastal mega-cities of developing nations, *Sustainable Cities and Society*, vol. 28, pp. 53-66. https://doi.org/10.1016/j.scs.2016.08.022

[11] Rana, D., S. Bichinepally, S. Kalra, A. Nandan, and N. A. Siddiqui. (2023) Comparative analysis of ultrafiltration for produced water from oil and gas industry, in *Advances in Waste Management*, N. A. Siddiqui, A. S. Baxtiyarovich, A. Nandan, and P. Mondal, Eds. Lecture Notes in Civil Engineering, vol. 301. Springer, Singapore. https://doi.org/10.1007/978-981-19-7506-6_7

[12] Fujita, C., M. S. Akhtar, R. Hidaka, et al. (2022) Mitigation of groundwater iron-induced clogging by low-cost bioadsorbent in open loop geothermal heat pump systems, *Applied Water Science*, vol. 12, p. 30. https://doi.org/10.1007/s13201-022-01574-x

[13] Nallakukkala, S. and B. Lal. (2023) Machine learning for scale deposition in oil and gas industry, in *Machine Learning and Flow Assurance in Oil and Gas Production*, B. Lal, C. B. Bavoh, and J. K. Sahith Sayani, Eds. Springer, Cham. https://doi.org/10.1007/978-3-031-24231-1_6

[14] Canny, J. (1986) A Computational approach to edge detection, *IEEE Transactions on Pattern Analysis and Machine Intelligence*, vol. PAMI-8, no. 6, pp. 679-698, https://doi.org/10.1109/TPAMI.1986.4767851.

[15] Suneetha, A. and E. S. Reddy (2020) Robust gaussian noise detection and removal in color images using modified fuzzy set filter, *Journal of Intelligent Systems*, vol. 30, no. 1, pp. 240-257. https://doi.org/10.1515/jisys-2019-0211

[16] Wedianto, A., H. L. Sari and H. Zuzaantri. (2016) Analisa perbandingan metode filter gaussian, mean dan median terhadap reduksi noise, *Jurnal Media Infotama*, vol. 12, no. 1. https://doi.org/10.37676/jmi.v12i1.269

[17] Chakrapani, Y. S., N. V. Rao, and M. Kamaraju. (2021) A survey of sobel edge detection vlsi architectures, *Journal of Physics: Conference Series*, vol. 1804, no. 1, p. 012151. https://doi.org/10.1088/1742-6596/1804/1/012151

[18] Rosenfeld, A. and A. Kak. (1976) *Digital Picture Processing*, p. 457. Academic Press.

[19] Kitchen, L. and A. Rosenfeld. (1982) Gray-level corner detection, *Pattern Recognition Letters*, vol. 1, no. 2, pp. 92-102. https://doi.org/10.1016/0167-8655(82)90020-4

[20] Smith, A. R. (1978) Color gamut transform pairs, *ACM SIGGRAPH Computer Graphics*, vol. 12, no. 3, pp. 12-19. https://doi.org/10.1145/800248.807361

[21] Su, C., Z. Li, Z. Wei, N. Xu, and Q. Yuan. (2023) Clarity method of low-illumination and dusty coal mine images based on improved AMEF, *Informatica*, vol. 47, pp. 51-62.

[22] Flores-Vidal, P. A., D. Gómez, J. Castro, and J. Montero. (2022) New aggregation strategies in color edge detection with hsv images, in *Information Processing and Management of Uncertainty in Knowledge-Based Systems*, D. Ciucci et al., Eds. Communications in Computer and Information Science, vol. 1602. Springer, Cham, https://doi.org/10.1007/978-3-031-08974-9_29.

[23] Heyns, P. S., R. Deetlefs, A. J. Oberholster, T. R. Botha, P. S. Els, and D. H. Diamond. (2020) Computer vision for rail surface defect detection, *Condition Monitor*, TN.403, pp. 6-10.

[24] Shafiabadi, M., A. Kamkar-Rouhani, S. R. G. Riabi, A. R. Kahoo, and B. Tokhmechi. (2021) Erratum to: Identification of reservoir fractures on FMI image logs using canny and sobel edge detection algorithms, *Oil & Gas Science and Technology*, vol. 76, p. 33. https://doi.org/10.2516/ogst/2021023

[25] Akter, Y. A., M. A. Rahman and M. O. Rahman. (2020) Quantitative analysis of mouza map image to estimate land area using zooming and canny edge detection, *TELKOMNIKA Telecommunication Computing Electronics and Control*, vol. 18, pp. 3293-3302. https://doi.org/10.12928/TELKOMNIKA.V18I6.16179

[26] Gunawan, G., H. Nuriyanto, S. Sriadhi, A. Fauzi, A. Usman, and F. Fadlina, et al. (2018) Mobile Application detection of road damage using canny algorithm, in *Proceedings of the 1st International Conference on Green and Sustainable Computing (ICoGeS)*, vol. 1019. Institute of Physics. https://doi.org/10.1088/1742-6596/1019/1/012035